A Dynamic Compensated and 95% High-Efficiency Supply Buffer in RGB Virtual Pixel MicroLED Display for Reducing Ghosting by 73% and Achieving Four Times Screen Resolution

Kai-Cheng Chung, Jia-Jyun Lee, Jia-Rui Huang, Yan-Jiun Lai, Ke-Horng Chen, *Senior Member, IEEE*, Ying-Hsi Lin, Shian-Ru Lin, and Tsung-Yen Tsai

***Abstract*—This article proposed micro light emitting diode (microLED) virtual pixel array design and driver. The proposed virtual pixel array effectively increases the pixels per inch and reduces parasitic capacitance for alleviating ghosting effects. The push-pull supply buffer in the proposed driver is compensated by the dynamic Miller compensation technique to achieve fast transient response and reduce the ghosting by 50%–73%. Four times screen resolution can be obtained compared to conventional designs. A 95% high-efficiency microLED driver has the lowest 45 μW power consumption. The proposed supply buffer can drive microLEDs in 51-inch display panel, which is composed of 214 small 96 $\times$ 64 microLED panels for automotive display.**

***Index Terms*—Dynamic Miller compensation (DMC) technique, microLED, virtual pixel array and driver.**

I. Introduction

INTERNET-OF-THINGS (IoTs) and wearable electronics that provide a compact solution for a variety of applications are becoming more popular. Limited by battery capacity, an efficient and compact form factor display is required [1]–[5]. Recently, micro light emitting diodes (microLEDs) have been more promising because they feature high-quality display with small volume and size. Some quality improvements are implemented to ensure that microLEDs can have state-of-the-art display resolution compared with other techniques [6]. The microLED display is composed of the thin-film transistor backplane, and the logic integrated circuit to control the LED emission [7]. In order to integrate red, green, and blue microLEDs in one panel, high-quality, high-resolution, full-color, and smaller pixel sizes are the development trend [8]. To ensure the driving uniformity, the LED current is also regulated by the constant-current source in the driver IC [9]. Thus, the driver IC can take the constant-current control of the analog signals and turn ON/OFF the microLEDs through the digital controller to achieve useful dimming functions.

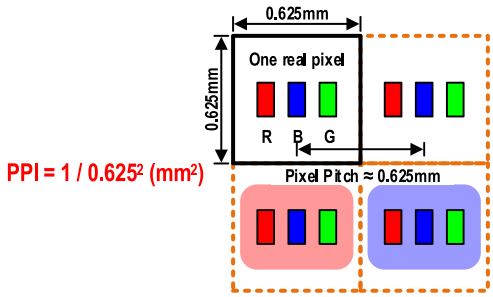

Fig. 1. Conventional microLED pixel design.

The microscopic LED array in the microLED display in Fig. 1 can much improve contrast, response time, and energy efficiency compared to an organic LED (OLED) display [1]–[2]. Mass transfer technology for microLED display continues to improve pixel resolution [3]–[5], but the design of pixel array in Fig. 1 is limited to pixels per inch (PPI) $= 1/0.625^2$ mm^2 because one pixel including a red (R), green (G), and blue (B) microLED occupies a footprint area of 0.625 x 0.625 mm^2. The distance between two adjacent pixels decides not only the PPI but also the parasitic capacitance value, C_{par0}–C_{par31}. To reduce hardware overhead, the microLED driver uses the time multiplexing technique to control the microLED array. However, during the row-by-row transition, the time multiplexing technique will suffer from the ghosting effect, which is mainly caused by the residual charge on C_{par0}–C_{par31}. As shown in Fig. 2(a), while row_0 is turning OFF from the ON-state, the voltage across the C_{par0} is less than V_{supply}. Since there is no path for electric charge to discharge, the voltage across C_{par0} can be kept less

Manuscript received May 26, 2020; revised September 21, 2020 and November 18, 2020; accepted December 19, 2020. Date of publication December 25, 2020; date of current version March 5, 2021. This work was supported in part by the Ministry of Science and Technology under Grants 108-2622-E-009 -007 -CC2, 106-2221-E-009 -165 -MY3, 106-2221-E-009 -095 -MY3, and 107-2321-B-468 -001. Recommended for publication by Associate Editor J. A. Cobos. *(Corresponding author: Ke-Horng Chen.)*

Kai-Cheng Chung, Jia-Jyun Lee, Jia-Rui Huang, Yan-Jiun Lai, and Ke-Horng Chen are with the Institute of Electrical and Computer Engineering, National Chiao Tung University, Hsinchu 300, Taiwan (e-mail: led3020@gmail.com; leejiajyun0508@gmail.com; jiarui_tw@yahoo.com.tw; j606331480521@gmail.com; khchen@cn.nctu.edu.tw).

Ying-Hsi Lin, Shian-Ru Lin, and Tsung-Yen Tsai are with the Realtek Semiconductor Corp., Hsinchu 300, Taiwan (e-mail: yslin@realtek.com; srlin@realtek.com; tytsai@realtek.com).

Color versions of one or more figures in this article are available at https://10.1109/TPEL.2020.3047372.

Digital Object Identifier 10.1109/TPEL.2020.3047372

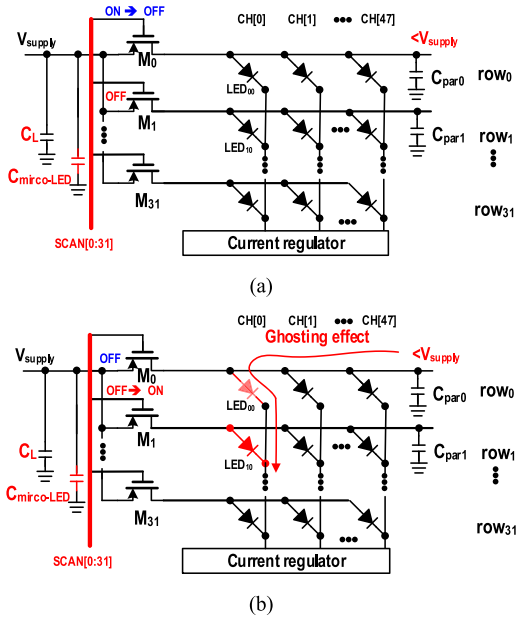

Fig. 2. (a) Residual charge is stored on the parasitic capacitance C_{par0} when the row_0 is turned OFF by setting SCAN[0] from low to high. (b) Ghosting effect occurs at the LED00 when SCAN[1] changes from high to low and CH[0] is turned on.

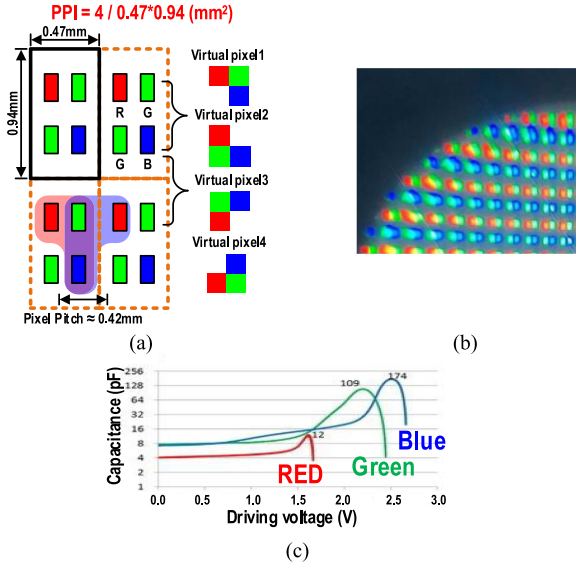

Fig. 3. (a) Proposed virtual pixel array. (b) Actual implementation of virtual pixel of microLED. (c) Capacitance variation of RGB microLEDs at different driving voltages.

than the voltage of V_{supply}, and there is little leakage. By the time-multiplexing method, if the row_1 turns ON and the channel CH[0] is also turned ON, the LED_{10} will emit light as expected. Meanwhile, an undesired side effect also occurs at the LED_{00} as illustrated in Fig. 2(b), because the residual charge on the C_{par0} finds a discharge path to turn ON the LED_{00}. The unexpected LED emitting light is the so-called ghosting effect.

The microLED display is plagued by ghosting, which is a serious problem in OLED displays. Therefore, to alleviate the ghosting effect to have a good display quality, this article modifies the pixel array design, arranges the driver control, and improves the transient response time of the supply buffer. In Fig. 3(a), two virtual pixels (virtual pixels 1 and 2) in the proposed microLED occupy an area of 0.94×0.47 mm^2. In addition, two additional virtual pixels (virtual pixels 3 and 4) in the vertical line can be derived to further increase the resolution. Each of the LEDs is used by four virtual pixels without increasing pixel area; thus, the virtual pixel array can have the advantage of four times higher screen resolution, as shown in Fig. 3(b), compared to the conventional pixel arrays. Thus, the overall parasitic capacitance can be reduced by 4. In scanning one row LEDs, the switching power loss is reduced by 4. In this work, the switching power loss occupies 1/3 of the whole driver. If the switching power loss can be reduced by 4, the overall power consumption can be improved by 25%. Moreover, the same color will be driven by the same microLED driver. Thus, the voltage difference between different colors can be minimized to eliminate the ghosting effect [10]. Although some external discharge circuits can be used to eliminate the ghosting effect in [10], the overall volume and size will reduce the attractiveness of microLEDs to today's displays. The conventional LED driver in [9] uses a step-up switching converter to generate a sufficiently high voltage to drive the microLEDs. Although the selectable feedback control can reduce the driving output variation, the step-up switching converter suffers from low bandwidth to react to the fast scanning change of microLEDs.

To alleviate the output-voltage ringing effect caused by parasitic capacitance changes, it is necessary to improve the drive capability and transient response time of the supply buffer. In Fig. 3(c), the capacitance of each color varies under different driving voltages. The capacitance variation ranges from 4 to 12 pF for the red microLED, from 8 to 109 pF for the green microLED, and from 8 to 174 pF for the blue microLED. Due to this change, the ratio of the maximum capacitance to the minimum capacitance is greater than 21.75. In addition, each microLED driver needs to turn ON 0–48 R, G, or B microLEDs, and the capacitance change may be as high as 8352 pF. To eliminate ghosting effects, the proposed push-pull supply buffer needs to provide sufficiently high bandwidth under wide output capacitance changes while maintaining high efficiency. Therefore, the ringing effect on the output voltage can be suppressed to avoid any ghosting effects.

The rest of this article is organized as follows. Section II shows the proposed microLED driver. The proposed microLED driver includes a push-pull supply buffer that is compensated by the dynamic Miller compensation (DMC) technique to ensure the adequate charging and discharging of the C_{par} by fast transient response. Circuit implementation is shown in Section III. Experimental results are shown in Section IV. Finally, Section V concludes the article.

II. Proposed MicroLED Driver

The driver IC of the virtual pixel microLED display is shown in Fig. 4, which delivers 1.6, 2.2, and 2.5 V different forward

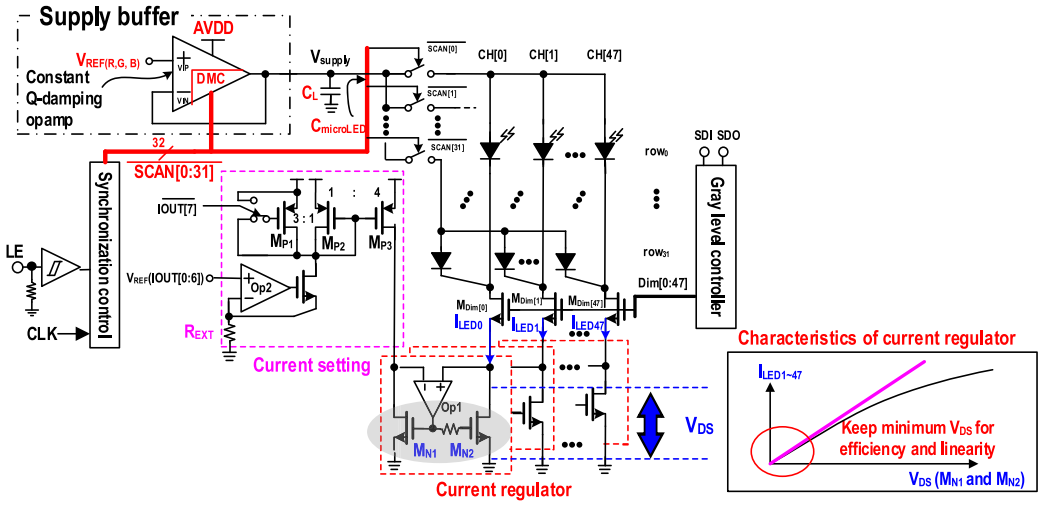

Fig. 4. Proposed microLED driver has the push-pull supply buffer, which is compensated by the DMC technique, and the current setting circuit to determine the current of the current regulator for driving the MOSFET in the triode region.

voltages for R, G, and B, respectively. The input voltage AVDD is regulated by the proposed push-pull supply buffer. The supply buffer consists a constant Q-damping operational amplifier and utilizes the DMC technique controlled by the scan line signal SCAN [0:31] to meet the minimum forward voltage of the R, G, and B microLEDs.

Owing to the limitation of small form factor in the microLED display, the filter capacitor C_L of the Q-damping operational amplifier needs to be limited within tens of picofarads, and the output pole will be located at high frequencies. However, when the microLEDs are turned ON, the capacitance will increase and the output pole will be pushed toward low frequencies to deteriorate stability. That is, the turning ON/OFF of a lot of microLEDs will have the stability issue if the supply buffer cannot rapidly react to the load changes. In order to solve the above problems, the scan signal SCAN [0:31] is compensated by the proposed DMC technique, which corresponds to an increase in the number of microLEDs that are turned ON.

The prototype of a 96 × 64 microLED panel requires eight microLED driver ICs to drive the R, G, and B microLEDs and the supply buffer provides an appropriate supply voltage accordingly. The gray level of each channel is controlled by a gray-level controller with 16-bit grayscale. The driving current setting is determined by the signal IOUT [0:7] and an external resistor R_{EXT}. The voltage headroom consumed by the current regulator determines the overall efficiency, and it is necessary to minimize the voltage drop across the current regulator. Therefore, the current regulator of Fig. 4 uses the operational amplifier Op1 to regulate the gates of M_{N1} and M_{N2}. Both M_{N1} and M_{N2} operate in the triode region to improve linearity and efficiency because they have the lowest V_{DS} voltage drop.

III. Circuit Implementation

The constant Q-damping operational amplifier in the proposed supply buffer includes three stages, as shown in Fig. 5(a). The input stage G_{m1}, from transistor M1 to M11, works as a folded cascade transconductance amplifier. The bias current of M1 and M2 is equal to that of the M4 and M5 to ensure similar slew rate for both positive and negative transitions. The second stage G_{m2}, formed by M12–M14, implements a positive transconductance that can establish the negative feedback from the last stage G_{m3}, which is a class-AB output amplifier that is driven by the common-gate MA and MB from the output current of the second stage.

The compensation stage G_{mD} consists of two parts, one part is used for N-type MOSFET MDN, whose gate is biased by the bias voltage VB5 through resistor R_{DN}, and the other part is used for P-type MOSFET MDP, whose gate is biased by bias voltage VB6 through the resistor R_{DP}. Both the drains of MDP and MDN are connected to the output of G_{m2}. The circuit can have a large swing without forcing MDP and MDN into triode region. The output total capacitance $C_{OUT(total)}$ $(= C_L + C_{microLED})$ increases with the number of microLEDs that are turned ON. In Fig. 5(b), the equivalent impedance Z_{eq1} consists of R_{DN}, C_{DN}, C_{DP}, R_{DP}, and the compensation stage G_{mD}. The other equivalent impedance Z_{eq2} is composed of R_{OUT}, $C_{OUT(total)}$, C_{D2N}, and the class-AB output stage G_{m3}. Z_{eq2} increases when $C_{OUT(total)}$ increases, and Z_{eq1} contains a constant compensation G_{mD}. The equivalent impedance provides the desired Z_{eq} $(= Z_{eq1} \parallel Z_{eq2})$, which is proportional to the square root of $C_{OUT(total)}$. As illustrated in Fig. 5(c), a constant Q-damping is established by the Z_{eq}. That is, the quality factor expressed in the following equation is constant at high frequencies. Thus, the constant Q-damping operational amplifier will not be affected by the increase of $C_{OUT(total)}$, as shown in Fig. 5(d)

$$Q = Z_{eq} \cdot \sqrt{\frac{C_{eq} G_{m2} G_{ms}}{C_{OUT(total)}}}. \quad (1)$$

For stability considerations, it is not necessary to design a constant Q-damping operational amplifier compensation at the maximum $C_{OUT(total)}$, thereby breaking through the bandwidth limitation and increasing the transient response. The supply

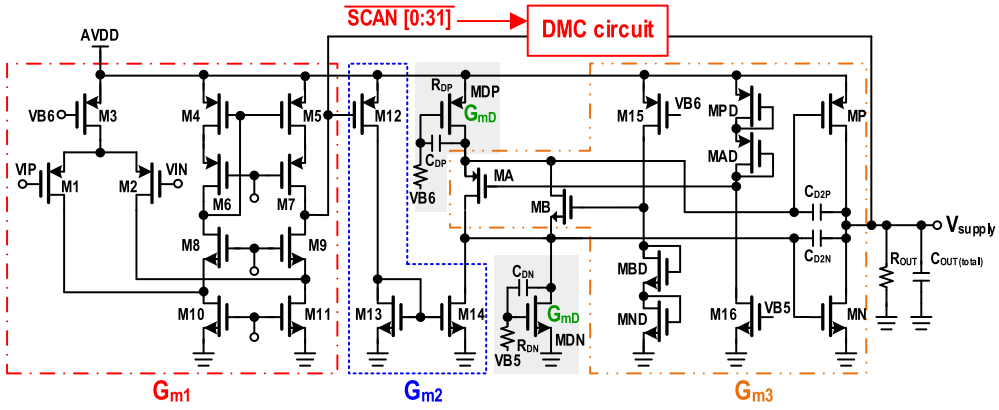

(a)

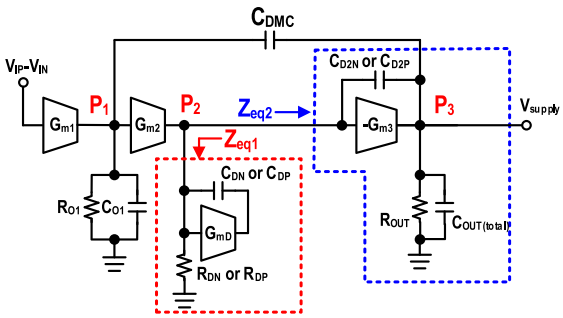

(b)

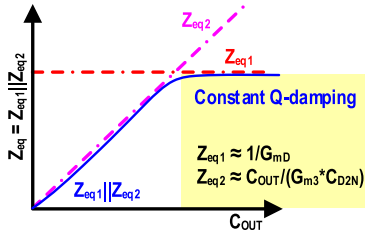

(c)

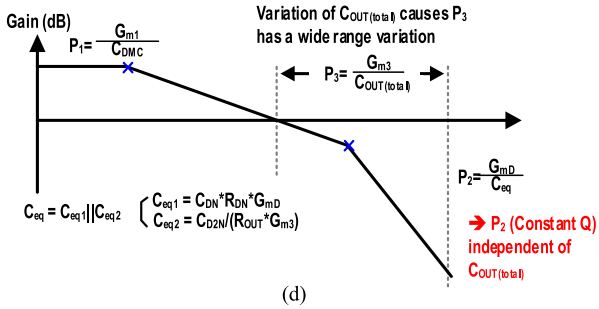

(d)

Fig. 5. (a) Operational amplifier of the supply buffer. (b) Small signal model of the operational amplifier. (c) Constant Q-damping is established by the R_{eq}. (d) Wide range GBW of the operational amplifier.

buffer can quickly change the drive capacity in response to the change of microLEDs that are turned ON. Although the parasitic capacitance will vary with the number of microLEDs that are turned ON, the Miller compensation can be adjusted adaptively to ensure stability without having any ringing effect at the output. In other words, even in the large capacitance change caused by the change between the minimum and maximum number of microLEDs that are turned ON, the supply buffer can be adaptively compensated through the DMC technique to improve stability.

Since $C_{\mathrm{OUT(total)}}$ is determined by the number of microLEDs that are turned ON, the scan line signal can turn ON or OFF the

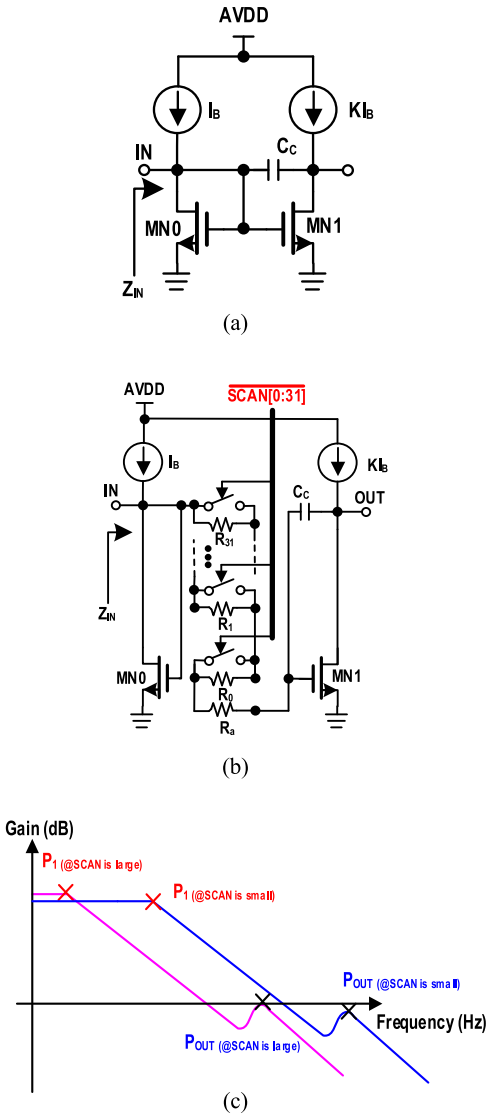

Fig. 6. (a) Conventional current mode Miller compensation. (b) Proposed DMC technique. (c) Increase GBW by the DMC technique.

microLEDs and at the same time control the Miller compensation in the DMC technique. In Fig. 6(a), conventional current mode Miller compensation uses the compensation capacitor C_C with an amplified current KI_B to derive a Miller equivalent capacitance $C_{\rm eq} = (1+{\rm K})C_C$. The derived input impedance $Z_{\rm IN}$ can be expressed as

$$Z_{\rm IN} = \frac{\left(1 + s\frac{C_C}{g_m}\right)}{sC_C(1+K)}. \tag{2}$$

Similarly, in Fig. 6(b), the DMC technique can add one series resistor with an equivalent $R_{\rm eq}$ in (3) controlled by the scan line signal SCAN [0:31] to control the equivalent capacitance $C_{\rm DMC}$ in (4) and derive the modified $Z_{\rm IN}$, as shown in (5). The switches in Fig. 6(b) are ON-chip MOSFET transistors fabricated in the same process as those in Fig. 4. It will have a small equivalent ON-resistance in parallel with the existing resistors R_0–R_{31} if the switch is turned ON. For example, if the scan signal SCAN [0] is high, the R_0 is used to increase the overall resistor value. Contrarily, if the scan signal SCAN [0] is low, a small ON-resistance contributed by the switch will be added to the overall resistor value. Although the small ON-resistance has little effect on compensation, it can be ignored.

When SCAN [0:31] has more logic "high," the $C_{\rm OUT(total)}$ is increased and more microLEDs are turned ON. Simultaneously, the value of $R_{\rm eq}$ is also increased by the SCAN [0:31]. Thus, the equivalent dynamic Miller capacitance $C_{\rm DMC}$ is also increased by the expression of (4). The dominant pole P_1, which is equal to $G_{\rm m1}/C_{\rm DMC}$, will be pushed toward the origin when $C_{\rm OUT(total)}$ increases. Contrarily, when $C_{\rm OUT(total)}$ decreases, SCAN [0:31] can decrease the value of $R_{\rm eq}$ and, thus, decrease $C_{\rm DMC}$. As shown in Fig. 6(c), the dominant pole P_1 can be pushed to a higher frequency to obtain a higher bandwidth to achieve a fast transient response. The DMC technique can ensure the stability of the entire drive circuit. The output of the supply buffer has no ringing effect and will not cause any residual charge on the output capacitor. In other words, the ghosting effect can be effectively suppressed

$$R_{\rm eq} = R_a + \sum_{i=0}^{31} R_i \cdot {\rm SCAN}[i]$$

$$\text{where } i = 0 \text{ to } 31 \tag{3}$$

$$C_{\rm DMC} = C_C \cdot (1+K) \cdot \left(1 + g_m R_{\rm eq} \cdot \left(\frac{K}{1+K}\right)\right) \tag{4}$$

$$Z_{\rm IN} = \frac{1 + sC_C\left(R_a + R_{\rm eq} + {}^1\!/_{g_m}\right)}{sC_{\rm DMC}} \tag{5}$$

IV. Experimental Results

The test chip was fabricated in a 0.15-μm CMOS BCD process. Fig. 7(a) shows the chip micrograph with an area of 4650 $\times$ 4580 μm^2. The microLED back-side driver system and the microLED front-side display are shown in Fig. 7(b). In Fig. 7(c), the proposed supply buffer can drive microLEDs in 51-inch display panel, which is composed of 214 small 96 $\times$ 64 microLED panels for automotive display.

Fig. 8(a) shows the ghosting effect on the channel CH[0] when SCAN [0] changes from high to low and vice versa. In the red microLEDs, if the transient voltage difference ΔV is higher than 1.6 V, the ghosting effect will be triggered as shown in Fig. 8(a). On the other hand, when the transient voltage difference ΔV is suppressed to 0.8 V due to the fast response of the proposed supply buffer in Fig. 8(b), the ghosting effect can be effectively suppressed. Moreover, the scan signal SCAN [0:31] can be pulled to low voltage not zero voltage to further reduce the ghosting effect where the low voltage can be programmed to be 1.7–2.2 V.

Similarly, the ghosting effect occurs when the transient voltage difference ΔV is higher than 2.2 and 2.6 V in green and blue microLEDs, respectively, as shown in Figs. 9(a) and 10(a), respectively. Due to the fast response of the proposed supply buffer, the transient voltage difference ΔV is suppressed to 0.8

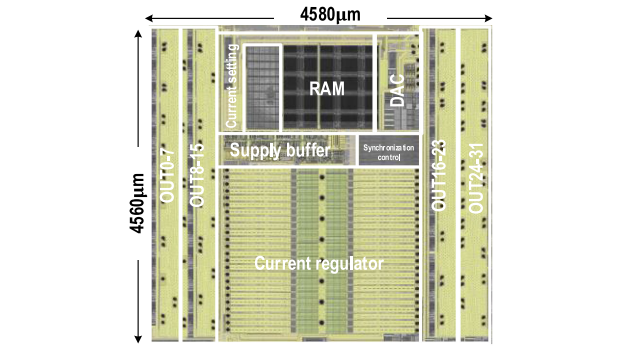

(a)

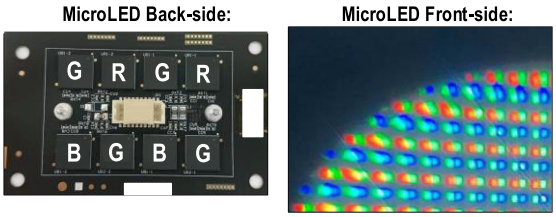

(b)

(c)

Fig. 7. (a) Chip micrograph. (b) MicroLED back-side (left) and front-side (right). (c) MicroLED has been implemented in 51-inch display panel for automotive display.

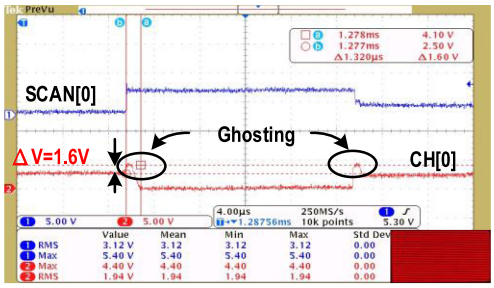

(a)

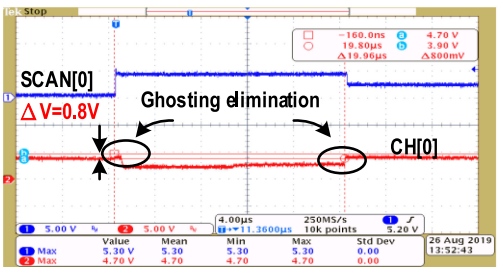

(b)

Fig. 8. Measured waveforms in the red microLED. The ghosting effect in (a) has been suppressed from 1.6 to 0.8 V in (b).

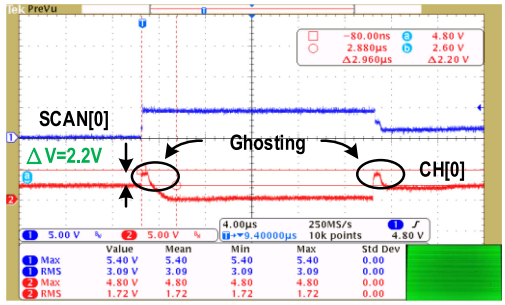

(a)

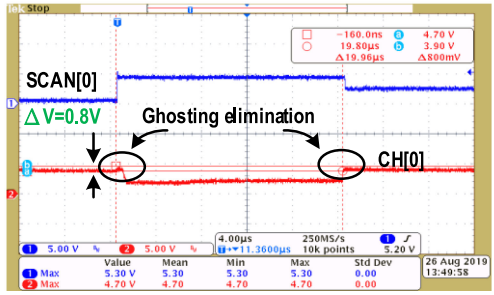

(b)

Fig. 9. Measured waveforms in the green microLED. The ghosting effect in (a) has been suppressed from 2.2 to 0.8 V in (b).

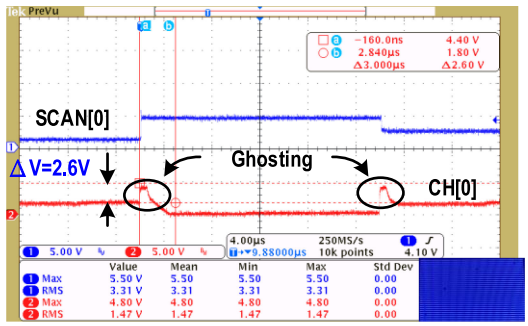

(a)

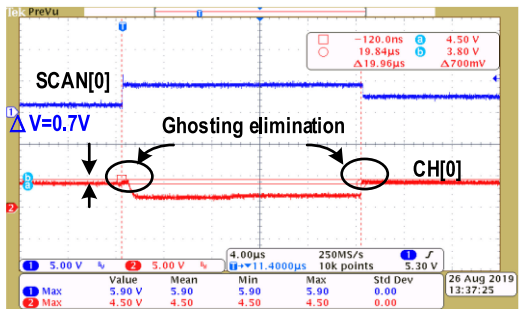

(b)

Fig. 10. Measured waveforms in the blue microLED. The ghosting effect in (a) has been suppressed from 2.6 to 0.7 V in (b).

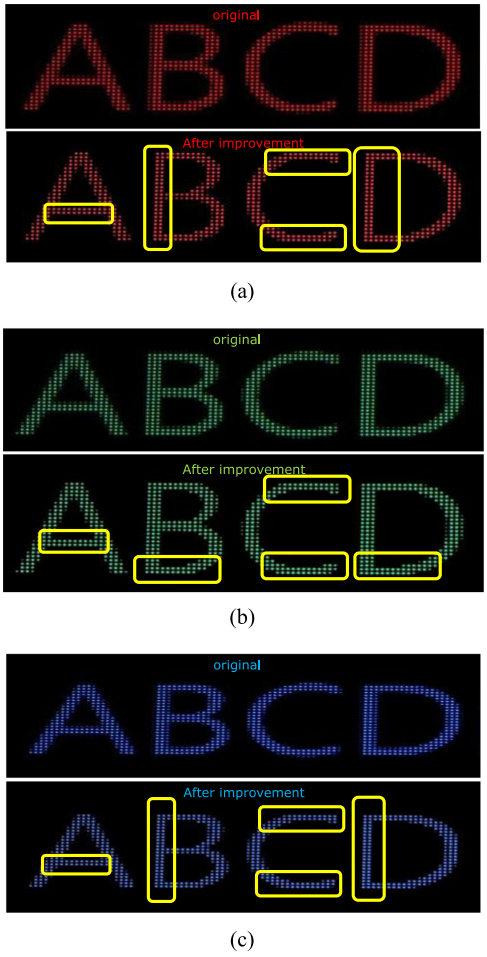

Fig. 11. Comparison of original picture and the improved picture without ghosting effect. (a) Red microLED display. (b) Green microLED display. (c) Blue microLED display.

and 0.7 V in green and blue microLEDs, respectively, as shown in Figs. 9(b) and 10(b), respectively. In conclusion, the transient voltage difference can be reduced by 50%, 64%, and 73% in R, G, and B microLEDs, respectively. In other words, the display quality can effectively be improved.

Fig. 11 shows the actual display of the original drive technique and the proposed supply buffer. The ghosting effect occurs at the edge of each letter in the original drive technique. After the proposed supply buffer improves the transient response, the ghosting effect can be effectively suppressed. Table I shows a comparison table between the proposed microLED driver and the prior arts of LED drivers.

Owing to the difficulty of measuring each channel power consumption, the power consumption is measured by scanning the whole screen to get the overall power consumption. During one frame time, the test turns ON each row of RGB microLEDs with their highest contrast in sequence to consume the maximum power. After that, turning OFF each row of RGB microLEDs in sequence tests the ghosting effect and measure the power consumption. The overall power consumption is divided by the number of channels to derive the power consumption of each channel. The proposed 95% high-efficiency microLED driver has the lowest 45 μW power consumption in comparison since the new proposed pixel design can effectively reduce the value of parasitic capacitance.

TABLE I
COMPARISON TABLE WITH THE PRIOR ARTS

	IEEE JSSC [1]	IEEE JSSC [2]	IEEE TCAS-II [3]	This work
Process technology	0.18μm CMOS	0.18μm CMOS	0.18μm CMOS	0.15μm CMOS
Application	AM-OLED	AM-OLED	MicroLED	MicroLED
Spatial resolution	UHD	QVGA:240*RGB*320	16*16*RGB	96*64*RGB
Gray scale	8bits	8bits	8bits	16bits
Source output range	1.5V-5V	0.2V-4.3V	N/A	0.05V-4.95V
1 LSB voltage	34mV	16mV	N/A	8mV
Available frame rate	60Hz	240Hz	120Hz	120Hz
Luminance deviation	0.4%	5.35%	0.91%	0.3%
Panel loads (R_L/C_L)	30KΩ /30pF	30KΩ /30pF	N/A/1pF	1KΩ/1pF
Power consumption (Per channel)	63.64μW	54μW	60μW	45μW

V. CONCLUSION

The proposed microLED display has four times screen resolution compared with conventional pixel arrays. The ghosting effect can be effectively suppressed since the pixel design reduces the parasitic capacitance and the driver is used for one color. Besides, the proposed microLED driver has a push-pull supply buffer that is compensated by the DMC technique to ensure fast transient response under the output capacitance variation from 1 to 8352 pF. For different R, G, and B microLEDs, the voltage difference ΔV to trigger ghosting effect is 1.6, 2.2, and 2.6V, respectively. After applying the proposed supply buffer, the voltage difference ΔV of the R, G, and B microLEDs is reduced to 0.8, 0.8, and 0.7 V, respectively, by 50%, 64%, and 73%, respectively. The ghosting effect can be effectively eliminated, although the ratio of the maximum capacitance to the minimum capacitance is greater than 21.75. The proposed 95% high-efficiency microLED driver has the lowest 45 μW power consumption in comparison.

REFERENCES

[1] J. Bang *et al.*, "A hybrid AMOLED driver IC for real-time TFT nonuniformity compensation," *IEEE J. Solid-State Circuits*, vol. 51, no. 4, pp. 966–978, Apr. 2016.
[2] H. Kim and D. Kim, "An active-matrix OLED driver CMOS IC with compensation of non-uniform routing-line resistances in ultra-thin panel bezel," *IEEE J. Solid-State Circuits*, vol. 53, no. 2, pp. 484–500, Feb. 2018.
[3] H. Ahn, S. Hong, and O. Kwon, "An active matrix micro-pixelated LED display driver for high luminance uniformity using resistance mismatch compensation method," *IEEE Trans. Circuits Syst. II: Express Briefs*, vol. 65, no. 6, pp. 724–728, Jun. 2018.
[4] J. Herrnsdorf *et al.*, "Active-matrix GaN micro Light-emitting diode display with unprecedented brightness," *IEEE Trans. Electron Devices*, vol. 62, no. 6, pp. 1918–1925, Jun. 2015.
[5] D. Peng, K. Zhang, and Z. Liu, "Design and fabrication of Fine-pitch Pixelated-addressed MicroLED arrays on printed circuit board for display and communication applications," *IEEE J. Electron Devices Soc.*, vol. 5, no. 1, pp. 90–94, Jan. 2017.

[6] K. Zhang, D. Peng, W. C. Chong, K. M. Lau, and Z. Liu, "Investigation of photon-generated leakage current for high-performance active matrix Micro-LED displays," *IEEE Trans. Electron Devices*, vol. 63, no. 12, pp. 4832–4838, Dec. 2016.
[7] C. Wei Lin, S. Ono, V. Gup, B. Mohammad, and V. Far, "Hybrid micro-driver architecture for driving microLED displays," U.S. Patent 10395590, Aug. 27, 2019.
[8] S. H. Yuan, S. S. Yan, Y. Yao, C. Wu, R. Horng, and D. Wuu, "Process integration and interconnection design of passive-matrix LED micro-displays with 256 pixel-per-inch resolution," *IEEE J. Electron Devices Soc.*, vol. 8, pp. 251–255, 2020.
[9] C. Hsieh, Y. Wei, K. Chen, and T. Lin, "Efficient LED driver with an adaptive reference tracking technique," in *Proc. 16th IEEE Int. Conf. Electron. Circuits Syst.*, 2009, pp. 291–294.
[10] Maxim Integrated, "Eliminating ghost-currents in color-LED display system using the MAX6972-MAX6975 LED drivers," Sept. 28, 2007, pp. 1–10. [Online]. Available: https://www.maximintegrated.com/en/design/technical-documents/app-notes/4/4111.html

Kai-Cheng Chung was born in Taipei, Taiwan. He received the M.S. degree from the Department of Electrical Engineering, National Central University, Taoyuan City, Taiwan. He is currently working toward the Ph.D. degree with the Institute of Electrical Engineering, National Chiao Tung University (NCTU), Hsinchu, Taiwan.

He holds more than 16 U.S. patents in the area of LED-circuit control design. His research interest interests include power system and micro-LED display designs.

Mr. Chung is a member of the Mixed-Signal and Power IC Lab, NCTU.

Jia-Jyun Lee received the M.S. degree from the National Chiao Tung University (NCTU), Hsinchu, Taiwan, in 2013. He is currently working toward the Ph.D. degree with the Department of Electrical and Computer Engineering, NCTU.

His research interests focus on power management integrated circuit designs.

Mr. Lee is a member of the Mixed-Signal and Power IC Lab, NCTU.

Jia-Rui Huang was born in Bhamo, Myanmar (Burma), in 1972. He received the B.Sc. and M.Sc. degrees from the Department of Physics, National Taiwan University, Taipei, Taiwan, in 1997 and 2005, respectively. He is currently working toward the Ph.D. degree with the Institute of Electrical Engineering, National Chiao Tung University (NCTU), Hsinchu, Taiwan.

After B.Sc. degree, he worked as a Research Assistant with the Institute of Atomic and Molecular Science, Academia Sinica, Taipei, Taiwan, and as an Advanced Technology Development Engineer for III-V compound semiconductor heterostructures and devices with Procomp Informatics Ltd., Hsinchu, Taiwan. He has more than 20 years of experience in semiconductor-related field. His research interests focus on power system designs and applications.

Mr. Huang is a member of the Mixed-Signal and Power IC Lab, NCTU.

Yan-Jiun Lai was born in Taipei, Taiwan. He received the B.S. degree from the Department of Electrical and Computer Engineering, National Chiao Tung University, Hsinchu, Taiwan, in 2016, and the Institute of Electrical and Computer Engineering, National Chiao Tung University, Hsinchu, Taiwan, in 2018.

He has authored two International Solid-State Circuits Conference papers from 2017 to 2018. His current research interests include the design of low-dropout regulator design, bandgap circuit design, and high-voltage operational amplifier designs.

Ke-Horng Chen (Senior Member, IEEE) received the B.S., M.S., and Ph.D. degrees from the National Taiwan University (NTU), Taipei, Taiwan, in 1994, 1996, and 2003, respectively.

In 2004, he joined National Chiao Tung University (NCTU), Hsinchu, Taiwan, having previously worked as an IC Designer in some IC design houses in Taiwan. He is currently a Professor and Chairperson of the Department of Electrical and Computer Engineering (ECE), NCTU, where he currently leads the Mixed-Signal and Power IC Lab, focusing on cutting-edge research on power management integrated circuit design. He and his research team at NCTU have been collaborating with many famous high-tech corporations, namely Realtek, Richtek, Novatek, etc., for more than ten years. His team has developed the first-ever design methodology of the SIMO converters improving silicon area and power efficiency and alleviating cross regulation problem. Recently, he has authored a textbook entitled *Power Management Techniques for Integrated Circuit Design* (IEEE Press and Wiley, 2016), which has been widely adopted as a textbook or design guide by students and engineers in Taiwan. He with his research group has authored or coauthored approximately 240 prestigious journal articles and conference papers. He has supervised 12 Ph.D. and 145 M.S. students. As the Chairman of the ECE Department, he manages the undergraduate program and three graduate programs including electrical and computer engineering, control engineering, and communications engineering, with 82 full-time and 16 adjunct staffs, 10 professional staffs, and 1423 students (705 graduate and 718 undergraduate students). He has led more than 80 academic-industrial collaboration projects receiving a total grant of more than 65 million TWD. In addition, their joint research efforts have been granted with more than 40 U.S. patents and more than 50 Taiwan patents. He is very active in IEEE and academic activities.

Dr. Chen is currently the Director of the Board of IEEE Taipei Section. He was the Chairperson of the Circuits and Systems (CAS) Society Taipei Chapter in 2015–2016 and also the recipient of the Outstanding Chapter Award of the IEEE Taipei Section. He has also been an Associate Editor for the IEEE TRANSACTIONS ON POWER ELECTRONICS since 2011, IEEE TRANSACTIONS ON CIRCUITS AND SYSTEMS I: REGULAR PAPERS since 2014, IEEE TRANSACTIONS ON CIRCUITS AND SYSTEMS II: EXPRESS BRIEFS in 2012–2013, and an Editorial Board Member of the Analog Integrated Circuits and Signal Processing since 2013. He has joined the Technical Program Committee of many important conferences including ISCAS (in 2010), ESSCIRC (in 2015), and CICC (in 2016). He is currently the General Co-Chair, organized the 2018 International Workshop on Power Supply on Chip (PwrSoC), the leading international technical workshop focusing on the integration of electrical power converters for multiple applications. He was the recipient of the Ministry of Science and Technology Outstanding Research Award in 2019 and the Outstanding Engineering Professor from Chinese Institute of Engineers in 2019.

Ying-Hsi Lin received the B.S. degree from National Chiao Tung University, Hsinchu, Taiwan, in 1993, and the M.S. degree in electrical engineering from National Taiwan University, Taipei, Taiwan, in 1995.

In 1995, he joined as a Researcher with the Computer and Communication Research Lab (CCL), ITRI, where he became a Project Leader of CMOS RF and high-speed mixed-signal circuits design in 1998. Since joining ITRI CCL, he has been working on CMOS radio frequency integrated circuits and mixed-signal circuits IC design for computer and communication application. In October 1999, he joined Realtek Semiconductor Corp., as an RF Manager, where he was responsible for several R&D CMOS RF projects including Bluetooth, WLAN 802.11abg, 802.11n, WLAN CE, and UWB, and also involving CMOS RF IC mass production planning. His research interests include circuit design include RF synthesizer, LNA, mixer, modulator, PA, filter, PGA, mixed-signal circuits, ESD circuits, RF device modeling, RF system calibration, and communication system design. He holds more than 30 patents in the area of mixed-signal and RF IC design. He has authored or coauthored eight International Solid-State Circuits Conference papers from 2015 to 2018.

Prof. Lin led the Research & Design Center of Realtek, where he became the Vice President in 2010.

Shian-Ru Lin was born in Nantou, Taiwan, in 1978. He received the B.S. degree from the National Taiwan University of Science and Technology, Taipei, Taiwan, in 2000, and the M.S. degree from National Taiwan University, Taipei, Taiwan, in 2003, both in electronic engineering.

In 2003, he joined the R&D Center of Realtek Semiconductor Corp., Hsinchu, Taiwan, where he is currently the Director. His current research interests include analog and mixed-mode circuit design, high-speed/resolution data converters, and timing recovery for communications, high-efficiency line driver, and power management IC.

Tsung-Yen Tsai was born in Pingtung, Taiwan. He received the B.S. degree from National Sun Yat-Sen University, Kaohsiung, Taiwan, in 2004, and the M.S. degree in communication engineering from National Chiao Tung University, Hsinchu, Taiwan, in 2006.

In July 2006, he joined Realtek Semiconductor Corporation, Hsinchu, Taiwan, as an Analog Circuit Designer. He is currently responsible for several projects including GPS, Bluetooth, WLAN802.11abg, 802.11n, and 802.11ac. His research interests include current DAC and switching regulators for SoC.